Review
The double-torsion testing technique for determination of fracture toughness and slow crack growth behavior of materials: A review

A. SHYAM, E. LARA-CURZIO*
Metals and Ceramics Division, Oak Ridge National Laboratory, Oak Ridge, TN 37831-6069, USA
E-mail: laracurzioe@ornl.gov

Published online: 15 June 2006

The double-torsion testing technique for fracture toughness and slow crack growth determination has been critically reviewed. The analytical compliance and finite element stress analyses of the double-torsion test specimen are summarized. The fracture toughness and crack growth testing procedure using this test configuration is described along with the applicable relationships. The strengths and limitations of this testing technique vis-à-vis other standardized techniques have been critically evaluated. While the double-torsion test method has some limiting features it has been demonstrated that its applicability is not limited as long as these are addressed correctly. Recommendations for conducting double-torsion experiments have been provided and potential avenues for improvement of this test method have been identified. It is concluded based on the review that standardization of this test method is required in order to make it more practicable.

1. Introduction

Double-torsion is a powerful testing technique for fracture mechanics characterization of materials. This testing methodology was introduced in the late 1960s [1, 2] and since then it has gained considerable popularity due to the relatively simple and inexpensive experimental set-up associated with it. The test configuration consists of symmetric four-point loading around a crack or a notch, on one end of a rectangular plate; this produces torsional deformation in the two plate halves. One distinguishing feature of this loading configuration is that the stress intensity factor is, at least as a first approximation, independent of crack length for a range of crack lengths in the test specimen. This implies that double torsion testing is ideally suited for the evaluation of opaque and non-reflective materials where crack length measurements could be difficult to make. For the same reason, the double-torsion set-up is amenable for testing in high temperature and controlled environments. Another reason for the popularity of the double-torsion test method, especially for slow crack growth studies, is the relative stability of crack extension. This is once again due to the fact that the stress intensity change at the tip of a growing crack in double-torsion is not nearly as dramatic as other testing configurations such as single edge notch bend (SENB) or compact tension (CT).

The mechanical properties that are evaluated by double-torsion testing include fracture toughness and slow crack growth behavior, although cyclic fatigue studies have also been reported. A wide range of materials have been characterized by double-torsion testing. These include ceramics (e.g. alumina [3–6], zirconia [7, 8], hydroxyapatite [9], mullite [10, 11], silicon nitride [12, 13], cordierite [14], silicon carbide [15–17]), glasses [18], composites [19–22], concrete and cement [23], Ni-base superalloys [24], steels [25], polymers [26–30], polycrystalline diamond [31], geological materials (e.g., lava rocks [32–34]), dry plaster [35], dental materials [36, 37], magnetic ferrites [38, 39], fuel cell materials [40], contact lens materials [41] and chemical vapor deposited diamond [42].

Good reviews of double-torsion testing are available in the literature and they are focused on the analytical [43], experimental [44] and practical aspects [45] of this test technique. These reviews and several investigators have stressed the importance of exercising caution when interpreting double torsion testing data, particularly because

*Author to whom all correspondence should be addressed.
0022-2461
DOI: 10.1007/s10853-005-5553-0

this test method has not been standardized. In recent years, several corrections have been proposed to the original analyses of the double-torsion test given by Evans and co-workers [25, 46]. Additionally, this testing technique is being applied to new materials and occasionally with modified configurations (e.g. [41]). In light of the above, the present review is organized in the following manner. The linear crack length-compliance analytical relationship that is the cornerstone of this test method and the expression for stress intensity factor will be discussed in the next section. This is followed by a review of finite element studies of this test configuration including recent studies that incorporate three dimensional analyses [47]. The methodology for fracture toughness and fatigue (static and cyclic) testing will be explained and the applicable relationships will be presented. The strengths and limitations of this testing technique have been critically evaluated. This is followed by a discussion of the relevant corrections that have been proposed to the conventional analysis of double-torsion in order to increase the accuracy of this test method. The overview is concluded with recommendations and identification of potential areas for further development of the double-torsion testing technique.

2. Analytical analysis of the double-torsion loading geometry

Fig. 1 is a schematic representation of the double-torsion test specimen while Fig. 2 is a picture of a double-torsion test specimen and loading fixture. Fig. 1a provides a schematic view of the test set-up and loading configuration. Early test specimen designs often included a groove along the length of the test specimen in order to guide the growth of the crack but recent work has shown that careful alignment of the test specimen and fixture obviate the need of the machined groove [45]. Furthermore, the presence of the groove leads to effects that are still not fully characterized and it also requires a modified analysis. Fig. 1b is a schematic drawing of a bar with a rectangular cross-section (after [25]) that represents the elastic torsional deformation in the halves around the cracked portion of the test specimen. If it is assumed that the two rectangular torsion bars in the test specimen deform independently and also that all displacements imposed on the test specimen exclusively generate torsional deformation in the individual bars, an analytical expression for the compliance of the test specimen can be obtained.

The total angle of twist (θ) resulting from a torque T on a circular bar with polar moment of inertia, I_p and shear modulus, G is given by the following expression [48]

$$\theta = \frac{TL}{GI_{\mathrm{p}}} \tag{1}$$

where, L represents the total length of the torsion bar. Derivation of a similar expression for bars of rectangular cross-section requires the application of the theory of elasticity. Williams and Evans [25] have shown that if the width of the test specimen (S) is much larger than its thickness (t) and if the length of any one of the rectangular bars is represented by the crack length (a), we obtain by recognizing that $T = (P/2)S_{\mathrm{m}}$, the torsional strain (θ) given by

$$\theta \approx \frac{\Delta}{S_{\mathrm{m}}} \approx \frac{3S_{\mathrm{m}}Pa}{St^3G} \tag{2}$$

where, Δ is the load-point displacement and its value is small compared to the moment arm S_{m} (the symbols have

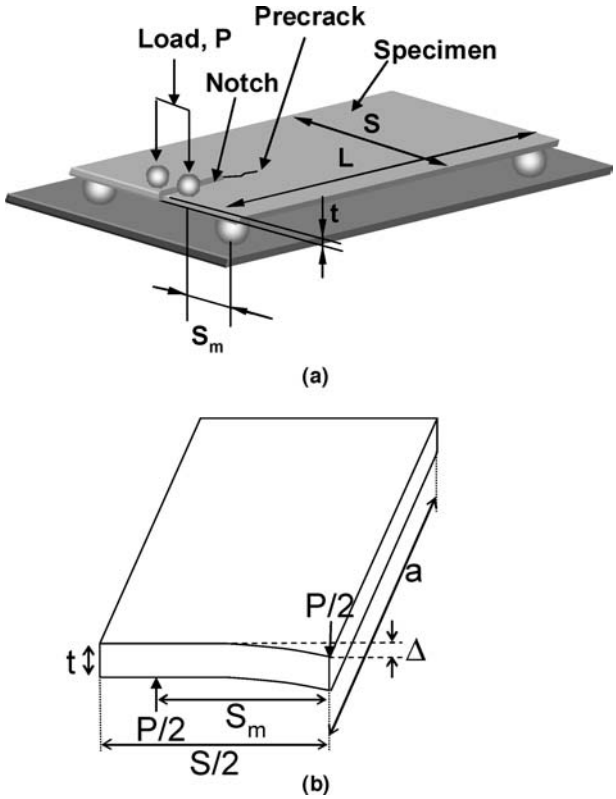

Figure 1 (a) A schematic view of the double-torsion test specimen and loading arrangement. (b) A schematic of the deformation in the individual rectangular bars.

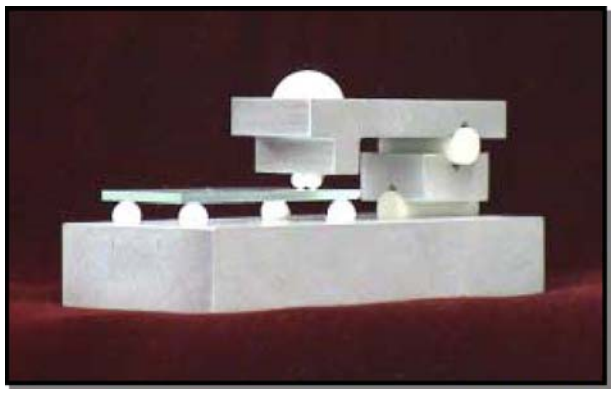

Figure 2 Example of an articulated test fixture and double-torsion test specimen.

been identified in Fig. 1). Equation 2 can be rearranged to give the analytical expression for the compliance (C) of a double-torsion test specimen

$$C \approx \frac{\Delta}{P} \approx \frac{3S_{\mathrm{m}}^2 a}{St^3 G} \tag{3}$$

Fuller [43] derived a more exact version of Equation 3 with a finite beam thickness correction factor $\psi(\tau)$ given by

$$C \approx \frac{3S_m^2 a}{St^3 G\psi\,(\tau)} \tag{4}$$

where, $\tau = 2t/S$ is the thinness ratio and for values up to $\tau = 1$, a simplified expression with an accuracy better than 0.1 percent is given by [43]

$$\psi = 1 - 0.6302\tau + 1.20\tau \exp\left(-\pi/\tau\right) \tag{5}$$

The validity of this thickness correction factor has been experimentally confirmed with the evaluation of glass ceramic test specimens [49]. This factor can be significant for thick beams (relative to width) and arises due to contact stresses between the two rectangular bars. If it is further assumed that the shape of the crack front remains unchanged as the crack propagates, then the following expression is obtained for the elastic strain energy release rate (G) [50]

$$\mathcal{G} = \frac{P^2}{2t}\left(\frac{dC}{da}\right) = \frac{3P^2 S_{\mathrm{m}}^2}{2St^4 G\psi} \tag{6}$$

where the Young's modulus is $E = 2G\ (1 + \nu)$, where ν is Poisson's ratio. With the application of the linear elastic fracture mechanics (LEFM) relationship [50]

$$K = \left(E'\mathcal{G}\right)^{1/2} \tag{7}$$

where, $E' = E/(1 - \nu^2)$ for plane strain and $E' = E$ for plane stress, the expression for stress intensity factor takes the following form

$$K = P S_{\mathrm{m}} \left(\frac{3}{St^4\,(1-\nu)\,\psi}\right)^{1/2} \quad \text{for plane strain} \tag{8a}$$

$$K = P S_m \left(\frac{3\,(1+\nu)}{St^4\psi}\right)^{1/2} \quad \text{for plane stress} \tag{8b}$$

The stress intensity factor given by Equation 8 is a function of the applied load, the test specimen geometry and Poisson's ratio but independent of crack length. The latter characteristic is one of the most attractive features of double-torsion testing. The independence of the stress intensity factor value with crack length, however, is valid only for a range of crack lengths in the double-torsion test specimen because edge effects lead to a deviation from the linear crack length-compliance relationship.

Experimentally, it has been found for several materials that the compliance varies with crack length in the following manner [25, 44, 46]

$$C = \frac{\Delta}{P} = Ba + D \tag{9}$$

where, B and D are scaling constants. The experimental form of the compliance relationship is slightly different from the expression in Equation 3. While this does not alter the form of the stress intensity relationship, it does have implications for slow crack growth measurements. The linear compliance-crack length relationship and other assumptions involved in the derivation of the analytical expression for compliance have been examined in Section 7. In the next section, these analytical expressions are compared to predictions obtained with finite element stress analyses of the double-torsion testing configuration.

3. Finite element stress analysis of the double-torsion loading geometry

The first comprehensive finite element stress analysis of the double-torsion test specimen was performed by Trantina [51]. This analysis concluded that most assumptions inherent in the derivation of the analytical expression are reasonable. The stress intensity factor calculation from the analytical analysis Equation 8 was shown to be nearly equal to the value obtained from the finite element stress analysis. Additionally, it was shown that the stress intensity factor remains nearly constant (to within 5%) in the range of crack lengths; $a > 0.55^*S$ and unbroken ligament lengths of $(L - a) > 0.65^*S$. This implies that the range of crack lengths for which the stress intensity factor is independent of the crack length is a function of the length to width (L/S) ratio of the test specimen. For $L/S = 2$, the middle 40% of the test specimen displays crack length independent stress intensity whereas for $L/S = 3$, the middle 60% of the test specimen displays this property.

More recently, Ciccotti and co-workers [32, 33, 47, 52] performed detailed three-dimensional finite element stress analyses for "large" double-torsion test specimens ($L > 17$ cm and $S > 6$ cm) and concluded that appreciable deviations occurred from the classical analytical solution predictions of strain energy release rate ($\mathcal{G}$ in Equation 6). They provided correction factors to account for experimental variables such as crack shape, groove width and depth, notch length and test specimen geometry and found deviations (up to 40%) in the value of strain energy release rate ($\mathcal{G}$) from the analytical solution [47]. Of all the effects considered, the effect of test spec-

imen geometry on the calculated stress intensity factor was found to be the most significant and complex. They provided tables of correction factors for various combinations of values of thickness (t): width (S): length (L). No general conclusions could be obtained from their analysis except that the discrepancies in stress intensity values predicted by analytical and numerical solutions decrease with decreasing the thickness of the test specimen [52]. Additional finite element studies on smaller sized test specimens having commonly used length to width ratio of 2:1 or 3:1 and dimensions representative of experimental double-torsion test specimens are necessary. This would help in standardized test specimen designs with well-defined operational range of constant stress intensity regions.

4. Double-torsion testing for fracture toughness determination

Fracture toughness can be determined in double-torsion testing simply by loading a pre-cracked test specimen rapidly and recording the maximum load at failure (P_{IC}). The fracture toughness expression is obtained by substituting the failure load in Equation 8

$$K_{IC} = P_{IC} S_m \left(\frac{3}{S t^4 (1-\nu) \psi} \right)^{1/2} \quad \text{for plane strain} \tag{10a}$$

$$K_{IC} = P_{IC} S_m \left(\frac{3(1+\nu)}{S t^4 \psi} \right)^{1/2} \quad \text{for plane stress} \tag{10b}$$

There are, however, some experimental aspects that need to be considered both during precracking and fracture toughness testing. The tip of the precrack should be in the region where stress intensity factor is independent of crack length. *A* small precrack leads to an artificially enhanced fracture toughness value and a small remaining ligament length results in a value lower than the fracture toughness of the material [44]. This can be avoided by making a starter notch with a length such that any crack that initiates from it is in the constant stress intensity region. It is important to conduct the fracture toughness test on a precracked test specimen since a blunt notch (without the precrack) would not allow equivalent stress intensification at the notch tip. Precracking is generally done at a slow crosshead displacement rate until a load drop can be discerned or a load plateau is reached where the increase in load is balanced by relaxation of the test specimen from crack growth. A notch with smaller width and a tapered end, such that it goes from full thickness to a thin ligament at the tensile surface, facilitates precracking at loads lower than P_{IC} [45]. Other methods of precracking, such as indenting the region in front of the notch to generate sharp pre-cracks contiguous to the machined notch, have also been successfully applied in double-torsion testing [3, 53]. The pre-crack originates from the tensile side of the double-torsion specimen and the shape of the resulting crack evolves before reaching a stable crack front. It is therefore desirable to reach the steady state crack front before performing fracture toughness or slow crack growth measurements. Depending on the material and specimen geometry, the stable crack front shape may be reached after 2–5 mm of pre-crack size ahead of the notch.

The determination of fracture toughness using a pre-cracked test specimen should be carried out at a fast loading rate so as to avoid slow crack growth. This is because slow crack growth prior to failure would lead to artificially lower values of fracture toughness. For example, it has been shown that the fracture toughness value of yttria stabilized zirconia (YSZ) increases with increasing crosshead displacement rates until a displacement rate of 4 mm/min and thereafter remains constant [54]. The experimental error in measuring the values of variables included in the formula for fracture toughness in double-torsion is comparable to that of six other geometries (chevron notched four-point bend, double cantilever beam, direct crack measurement, single edge notched tension, single edge notched specimen tested in three-point bend and single edge notched tension, single edge notched specimen tested in four-point bend) and better than indentation strength by four-point bending [55]. In summary, double-torsion testing provides fracture toughness values comparable to those obtained from other standardized test methods provided the above-mentioned experimental requirements are satisfied.

5. Double-torsion testing for crack growth study

One of the most important characteristics of the double-torsion testing approach is that the rate of slow crack growth can be derived without having to monitor the crack length on a continuous basis. Additionally, the cyclic fatigue crack growth response of a material can be determined if crack length is monitored continuously. The initial analyses for load relaxation and constant displacement rate techniques were given by Evans [46] although several corrections have since then been proposed to refine that approach (Section 8). We describe in the present section, four commonly employed procedures for crack propagation studies with the double-torsion testing configuration.

5.1. Load relaxation technique

The load relaxation technique [46] is commonly employed to indirectly obtain the sub-critical crack propagation behavior of brittle materials. According to this technique, a pre-cracked double-torsion test specimen is loaded to below the expected fracture load (0.90–0.95$*P_{IC}$). The crosshead of the testing machine is then held at a fixed position and the increase in compliance of the test specimen from sub-critical crack growth leads to a relaxation of the load with time. To illustrate this concept, Fig. 3

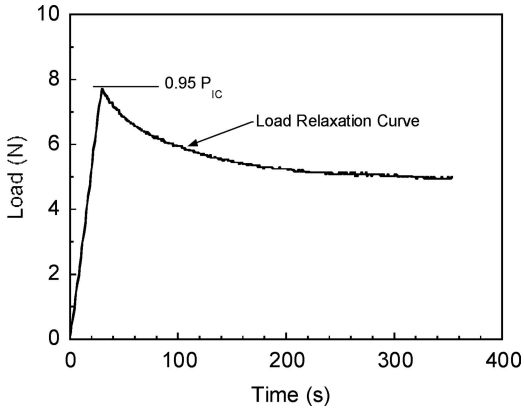

Figure 3 An illustration of temporal load variation obtained from a load relaxation test in a double-torsion test specimen of 3-YSZ.

presents a load relaxation curve for a test specimen of 3-YSZ. Mathematically, this can be described by differentiating Equation 9 with respect to time to obtain the following relationship

$$\frac{d\Delta}{dt} = (Ba + D)\frac{dP}{dt} + PB\frac{da}{dt} \tag{11}$$

where, the left hand side (LHS) of the equation equals zero if the crosshead is arrested. Additionally, if Δ remains constant, and the tip of the crack remains in the crack length independent stress intensity region, then

$$P\,(Ba + D) = P_i(Ba_i + D) = P_f\left(Ba_f + D\right) \tag{12}$$

where, the subscripts '*i*' and '*f*' denote the initial and final loads and crack lengths. The physical meaning of Equation 12 is that the increase in the compliance of the test specimen due to increase in crack length is exactly compensated by its temporal decrease in load. By setting the LHS of Equation 11 equal to zero and rearranging it with Equation 12, an expression for the crack growth velocity ($v = da/dt$) can be derived

$$v = \frac{-P_i}{P^2}\left(a_i + \frac{D}{B}\right)\frac{dP}{dt} \tag{13}$$

which reduces to the following simplified expression for the case $a_i \gg (D/B)$, i.e. large crack lengths or high modulus materials

$$v = \frac{-a_i P_i}{P^2}\frac{dP}{dt} \tag{14}$$

Even though Equation 14 is popularly applied, it is noted that in many cases the assumption that a_i is much larger than (D/B) is not true. Equation 14 should be applied when material availability is at a premium and experimental compliance-crack length curves cannot be generated. However, the slow crack growth exponents calculated using Equations 13 or 14 will remain identical. For a given load and average velocity, the corresponding stress intensity value can be calculated from Equation 8. In principle, the entire v-K curve can be obtained from a single load relaxation experiment. In practice, however, this methodology works better at relatively higher crack growth rates ($>10^{-6}$–10^{-7} m/s [44]) due to temperature fluctuations affecting load measurements at very low velocities. This method is also susceptible to spurious factors, such as load train relaxation, which is discussed further in Section 7. It is for this reason that it has been recommended to generate complementary portions of the v-K curve by combining the load relaxation technique with one of the two techniques discussed below [56].

5.2. Constant load technique

The earliest application of the double-torsion loading configuration to measure slow crack growth was through the constant load method [57]. The average crack velocity corresponding to the stress intensity factor, which is calculated from the applied constant load, can be obtained by measuring the crack length before and after the experiment and the elapsed time. The main disadvantage of this technique is that only one data point can be obtained per experimental run since crack length measurements are required. This technique, however, is suitable for the calculation of very low crack velocities where load relaxation measurements cannot be performed [44]. Additionally, at elevated temperatures, inelastic deformation and machine relaxation render constant load crack growth measurements as the most reliable technique to measure slow crack growth rates [44].

5.3. Constant displacement rate technique

Evans [46] introduced another technique for evaluating slow crack growth behavior that involved changing the displacement rate incrementally. In this technique, the crosshead is moved at a constant rate and the load value is allowed to reach a plateau where the increase in load from crosshead movement is balanced by relaxation of the test specimen load from crack growth. If the plateau load value is given by P, Equation 11 reduces to the following form (with $dP/dt \sim 0$)

$$\frac{d\Delta}{dt} = PBv \tag{15}$$

The crack velocity can be calculated from the displacement rate and the value of the load plateau. The main disadvantage of this technique is also that only one data point can be obtained per test run even though crack length measurements are not required. By changing the displacement rate over a few decades, Evans showed that the slow crack growth exponent can be determined from this testing methodology [46].

Weiderhorn [58] and later Quinn and co-workers [3, 59] successfully combined the constant displacement

rate technique with the load relaxation technique to obtain slow crack growth information without having to make any crack length measurements. In this method, the crosshead is moved at a slow, constant rate until the load decrease due to slow crack growth exactly offsets the load increase due to crosshead movement. The peak load (P_i) and the crosshead displacement rate ($d\Delta/dt$) can now be used to obtain the crack velocity (v_i) according to Equation 15. In this version of the test method, the crosshead is arrested at the peak load and a load relaxation experiment is subsequently carried out. The initial crack velocity (v_i) from the load relaxation experiment can be obtained by substituting $P = P_i$ in Equation 13. Assuming that the initial velocity obtained by application of Equations 13 and 15 is the same, the following relationship is obtained:

$$v_i = \frac{(d\Delta/dt)}{P_i B} = -\left(\frac{dP_i}{dt}\right)\frac{(Ba_i + D)}{P_i B} \qquad (16)$$

This relationship allows the expression of the compliance of the specimen at the beginning of the load relaxation experiment as [58]

$$Ba_i + D = -\frac{(d\Delta/dt)}{(dP_i/dt)} \qquad (17)$$

The initial compliance is related to the compliance at any other instant in the load relaxation experiment according to Equation 12. Substitution of Equation 17 in Equation 13 therefore, allows the calculation of crack velocity according to

$$v = \left(\frac{d\Delta/dt}{B}\right)\left(\frac{P_i}{dP_i/dt}\right)\left(\frac{dp/dt}{P^2}\right) \qquad (18)$$

Since Equation 18 does not involve any crack length term, it is ideally suitable for applications such as elevated temperature and/or controlled environment testing.

5.4. Cyclic fatigue crack growth measurements

There have been few reports of cyclic fatigue studies using the double-torsion testing methodology [45, 60–62]. This is due to the fact that cyclic fatigue studies typically require continuous monitoring of crack length with loading cycles, e.g. [61]. In principle, the crack length in a double-torsion test specimen can be estimated from the compliance of the test specimen. However, it has been reported that accurate determination of the crack length from the compliance of the test specimen can be difficult in practice, especially for brittle materials [45]. This is attributed to the small load point displacements associated with the deformation of stiff materials and the inherent noise associated with thermal fluctuations, for example. Chevalier and co-workers [53, 61, 63–69] have extensively studied the static and cyclic crack growth behavior of zirconia using the double-torsion configuration. Using this testing approach they found the existence of thresholds for crack growth (in both static and cyclic conditions) and the presence of environmentally-assisted degradation mechanisms [61]. It has also been demonstrated that a cyclic effect exists in several materials in terms of faster crack growth at equivalent value of stress intensity factor when compared to stress corrosion alone [61, 62]. A cyclic effect may also exist in that the crack propagation threshold values are lower under cyclic fatigue loading [61].

6. Advantages of the double-torsion testing technique

Some of the advantageous characteristics of the double-torsion testing configuration for fracture toughness and slow crack growth characterization have already been identified in the previous sections. The simple test specimen geometry and loading configuration involving four-point loading of a rectangular bar results in a low-cost setup [43]. Even the rear supports of the test specimen (Fig. 1) are not critical since they are designed only for convenience in mounting and aligning the test specimen [25]. The most important characteristic of this testing configuration, as mentioned earlier, is that the stress intensity factor resulting from it is independent of (or has a weak dependence on) the crack length in the mid-section of the test specimen. The above factors are responsible for the fact that the application of this test method is commonly extended to elevated temperatures and controlled environments, e.g. [15]. In addition, it has been noted that a low compliance loading system is not required to apply the compressive loads required for double torsion testing [34]. Although the tapered width double cantilever beam test specimen also has the property of the stress intensity factor being independent of crack length, these test specimens require a lot more material for machining compared to a flat double-torsion test specimen [70]. The double-torsion test specimen geometry is also ideally suited for material manufactured in a planar configuration such as polycrystalline diamond compacts [31]. This testing configuration is also uniquely suitable for determining the fracture toughness of rocks [33], adhesive joints [71] and diffusion bonds [72].

In double-torsion test specimens, precracking is achieved in a controlled manner and can be detected from deviations from linearity in the load versus displacement curve [43]. Unlike double-torsion, some other geometries for measuring fracture toughness involve separate fixturing for precracking test specimens (e.g. the precracked beam method).

Some researchers have claimed that values of the fracture surface energy calculated from double-torsion (DT) testing are more accurate when compared with other configurations such as double cantilever beam (DCB) or sin-

gle edge notch bend (SENB) testing [73]. Others have reported comparable values of fracture energy release rates obtained by DT and DCB test specimens [74] whereas others have reported that the DCB test specimen geometry has the highest tendency for slow crack growth and yields higher values of fracture toughness compared to SENB or DT test specimen geometries [75]. For hot-pressed SiC, for example, comparable K_{IC} values were reported from Hertzian indentation and double-torsion techniques [76]. However, uncertainties in the fracture toughness determination from indentation techniques are well documented and therefore fracture toughness values from double-torsion are deemed more reliable than those attempted from indentation methods [54].

As mentioned in Section 5, slow crack growth can be investigated in three complementary modes using double torsion without the use of crack opening displacement gages. Evans and Williams [25] have demonstrated that slow crack growth characteristics are extremely comparable for several materials using the DT and DCB test specimen configurations. Bhaduri [18] reported that the slow crack growth exponent calculated from indentation techniques is comparable to that calculated from double-torsion. While studying stress corrosion cracking in steels, Briggs *et al*. [77] found that an optical method for measuring crack growth rates and the load relaxation version of the double-torsion test method gave similar results. Quinn and Quinn [59] carried out a comparison of the published slow crack growth exponent values in hot pressed silicon nitride between room temperature and 1400°C. They demonstrated that in some instances, the slow crack exponent values were similar between double-torsion and other test methods such as static and dynamic fatigue. Quinn [3] also demonstrated the coincidence of the slow crack growth exponent between double torsion and static fatigue testing for alumina at 1000°C. Slow crack growth characteristics calculated from static/dynamic fatigue experiments are indirect calculations whereas in the double-torsion test the slow crack growth behavior of long cracks can be deduced directly [9]. It has been shown by Sudreau *et al*. [78] that indirect methods can induce large errors in interpretation of slow crack growth characteristics. Double torsion has also been successfully applied to investigate the time dependant fracture of composite materials [19, 20] and tough polymers [21].

7. Limitations of the double-torsion testing technique

It is important to be aware of the major assumptions involved in double-torsion testing that could limit its validity under certain circumstances. One assumption involves the choice of state of plane strain or stress to describe the stress intensity at the crack tip according to Equation 8a or 8b. While earlier researchers favored the plane strain expression for fracture toughness calculation [43,45] recent calculations are based on the plane stress expression,

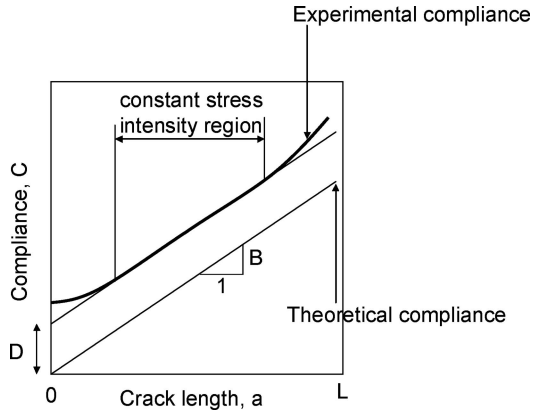

Figure 4 The experimental variation of compliance with crack length in a double-torsion test specimen leads to the mid-region in the test specimen with stress intensity values independent of crack length. The theoretically predicted compliance variation with crack length has also been illustrated in this figure.

e.g. [40]. The justification for the former is that plane strain fracture toughness is suitable for brittle materials. Fracture modality selection (plane stress/strain) can induce errors in the calculation of the stress intensity factor according to Equation 8. The other assumption is that the loading at the tip of the crack is purely mode *I* with a negligible mode III component [43]. This was shown to be a reasonable assumption by Evans and co-workers [25, 46], who demonstrated the experimental critical strain energy release rate (G_c) compared well with mode *I* values calculated from Equation 7.

The most important characteristic of the double-torsion test specimen is the lack of dependence of the stress intensity factor on crack length in approximately the mid-range of crack lengths in the test specimen. Outside this region, the compliance-crack length relationship becomes nonlinear due to end effects and this has been schematically illustrated in Fig. 4 [43]. One assumption in the analytical derivation of this relationship is that the torsion bars deform independently with no contact stresses and negligible deflection beyond the crack tip. The reason for the slopes of compliance versus crack length curve (Fig. 4) becoming lower than that of the constant slope region at smaller crack lengths is due to interaction between the two torsion bars in the test specimen contributing significantly to the total deformation of the torsion bars [25]. At small remaining ligament lengths, the elastic deflection of the uncracked portion of the test specimen does not remain negligible thus increasing the slope of the compliance-crack length curve in Fig. 4. Even for the so called region of constant driving force, a number of researchers have found that the stress intensity factor could be a function of the crack length [4, 5, 14, 44, 56, 63, 64, 79, 80]. Very often, a hysteresis in the v-K curve calculated from load relaxation is shown as indication of the dependence of stress intensity factor on crack length [44, 56, 63, 64, 79, 80]. The dependency of stress intensity factor on crack length has been attributed

to several factors which can be broadly classified as follows:

- Intrinsic effects—These effects arise from the material microstructure or the interaction of the material with the environment. Example of such effects would be the presence of a glassy phase on the grain boundaries [79], transformation toughening at the crack-tip [53, 81], time dependant deformation in the process zone [56] and R-curve effects such as friction induced bridging of grains, reinforcements from fibers or phase transformations [5, 6, 56].
- Extrinsic effects—These effects are due to the mechanical evolution of the stress intensity factor with crack growth. Use of Equation 8 to calculate the stress intensity factor may, therefore lead to errors. In such situations, finite element stress analysis or alternative approaches (see Equation 20 in Section 8) are required to calculate the stress intensity factor. An extrinsic effect could arise from the uncracked compressive portion of the double-torsion test specimen [63].

In addition, the crack profile in double torsion is curvilinear and therefore, the stress intensity factor is expected to vary along the crack front. It has been contended that the crack front geometry is material specific [82] and dependent on the slow crack growth exponent [83]. Researchers have argued that the shape of the crack front does not change in the constant stress intensity region [25, 29, 84] and therefore a crack shape correction factor can be used to correct for these effects (see Section 8).

The geometry of the double-torsion test specimen has not been standardized and in some cases this might lead to the crack propagation characteristics influenced by the test specimen dimensions [44, 60]. For example, it is known that a test specimen with thickness greater than (S/6) can lead to an interaction between the two moment arms that can not be neglected [44, 85]. It is also known that the region of constant stress intensity decreases in size if the length to width ratio of the test specimen decreases [85, 86]. Large deflections or big roller pins also change the effective moment arm length of the test specimen as discussed in the next section [30]. Quinn and Quinn [59] demonstrated that surface finish had an effect on the results of double-torsion experiments on a large Plexiglas test specimen. Most of the recent applications of double-torsion testing have been carried-out using test specimens without a guiding groove, and rightly so, since the additional stress concentration due to the groove leads to effects that are not well understood [45]. The crack is likely to not remain straight and wander if the loading system is not well aligned and balanced.

As mentioned earlier, the load relaxation method can be affected by spurious effects [44, 56, 79]. This is especially true in situations involving substantial machine relaxation, very low crack velocities [44], high temperature and crack-tip plasticity [11]. The problem can be

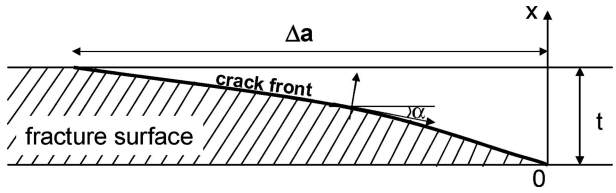

Figure 5 A schematic of the cross section of a crack in a double torsion test specimen showing the curved crack front. Geometric corrections associated with the curved profile have been proposed [46, 84]. The intersection angle of the crack with the tensile surface has been exaggerated in this figure.

partially circumvented by subtracting the background relaxation of the system or alternately by using the constant load technique [44]. The errors due to end effects can artificially decrease the slope of the v-K plot or the slow crack growth exponent by as much as 30% [52, 86]. If extrinsic effects are significant, even in the so called "constant driving force regime", a systematic error in the slope of the v-K plot up to 50% can be observed [63]. Additional corrections in the slow crack growth rates need to be applied in the presence of crack bridging [12], blunting, branching and deflection [87]. We discuss in the following section, corrections that have been proposed to the conventional analysis of double torsion in order to address some of the problems discussed in this section and thereby increasing the precision of this testing method.

8. Corrections proposed to the conventional analysis of double-torsion

Several corrections have been proposed for the quantitative analysis of data obtained by the double-torsion test method. One of the most relevant corrections, for slow crack growth studies, has been for the curvilinear crack profile schematically illustrated in Fig. 5. Since the crack extends further along the face of the test specimen with the maximum tensile stress, Evans [46] proposed the following first order correction for the effect of crack profile on velocity given by Equation 14

$$v = \phi \frac{-a_i P_i}{P^2} \frac{dP}{dt} \tag{19}$$

where, $\phi = t/\sqrt{(t^2 + \Delta a^2)}$ with t representing the thickness of the test specimen and Δa the difference in crack lengths between the two faces (Fig. 5). This correction approximates the curved crack front with a straight line. Shetty, Virkar and Harward [88] pointed out that since the crack front is curved and the crack velocity is defined orthogonal to the crack front, the velocity must decrease continuously along the front starting from a maximum value at the leading edge. Based on the curved crack profile, they derived an expression for the average crack velocity as a weighted average of the components of the local velocities along the average direction [88]. Pollet and Burns [84] provided the most accurate expression to correct crack velocity values due to the crack front curva-

ture. If the angle between the test specimen surface and the normal to the crack front is locally given by α (Fig. 5), then the crack velocity correction (ϕ in Equation 19 can be shown to be [84]

$$\phi = \left[\frac{1}{t} \int_0^t \{\sin \alpha\,(x)\}^{1/n} dx \right]^n \tag{20}$$

where, t is thickness of the specimen, n is the slow crack growth exponent and the expression for ϕ reduces to the correction proposed by Evans [46] if the crack front is approximated as a straight line with α remaining constant. The value of ϕ can be obtained from experimental measurements of the crack profile. Ciccotti and co-workers [32, 33, 47, 52] performed finite element simulations incorporating geometric features such as the relative test specimen dimensions and the curved crack front to provide tables from which a linear corrective factor could be obtained. This factor could be applied to conventional analysis [46] of slow crack growth with the double-torsion testing method.

The correction to the stress intensity factor based on the thickness of the beam relative to its width has already been discussed Equation 8. Hine, Duckett and Ward [89] extended this thickness effect by correcting for large deflections and the size of the moment arm in case of finite radii of the loading points. Their analysis yielded the following expression for stress intensity factor, for the case of plane stress

$$K = P \left(\frac{3\Delta\,(1+\nu)}{St^4\psi} \right)^{1/2} \times \left[\frac{S_m - (R + r + t)(\sin\theta + \theta\cos\theta)}{\theta} \right]^{1/2} \tag{21}$$

where the terms have the same meaning as in Equation 8. In addition, Δ represents the crosshead displacement, R and r are the radii of supporting and loading balls and θ is the angle the torsional arm makes with the horizontal surface of the undeformed test specimen. Equation 21 reduces to Equation 8b for the case of small values of radii R and r with small deflections where $\Delta \sim S_m\theta$. The issue of large deflection in double-torsion has been theoretically [90,91] and experimentally [30] addressed by researchers investigating the behavior and properties of polymers and polymer based composites.

The standard rectangular double-torsion test specimen configuration and analysis has been reported to be modified by investigators for specialized applications. McAuliffe and Truss [41] tested semi-circular test specimens made from polymeric ophthalmic contact lens material and demonstrated that the fracture toughness, for the case of plane stress, was given by

$$K_{IC} = P_{IC} S_m \left(\frac{3\,(1+\nu)}{(r^2 - a^2)t^4} \right)^{1/2} \tag{22}$$

where r is the radius of the test specimen and a is the crack length and the thickness correction factor has been ignored. As might be expected, material specific considerations are commonly applied to modify the analytical expressions for double-torsion outlined in the previous sections. For example, Donners and co-workers [38 , 39] while studying the fracture of MnZn ferrites demonstrated that the expression for fracture toughness is a function of the environmental conditions and determined by the adsorption or reactive species on the crack tip. Radovic and Lara-Curzio [40] have demonstrated a clear relationship between porosity of materials for solid oxide fuel cell applications and their fracture toughness. The variation in the local crack-tip driving force based on deflection of the crack tip during a double-torsion experiment has also been addressed [87].

Chevalier and co-workers have reported in a series of papers [61, 63–68, 92] a crack length dependence of stress intensity factor while studying the behavior of zirconia and alumina. According to them, the corrected expression for stress intensity factor (K_{corr}) in the double-torsion testing configuration can be given by

$$K_{corr} = K \left(\frac{a}{a_o} \right)^{m/k} \tag{23}$$

where K is given by Equation 8, a_o is the notch length, $m = 6$ and $k = 32$ are constants for the test specimen geometry and material considered. They have attributed the minor crack length dependence of stress intensity factor to the unbroken ligament on the compressive side of the test specimen and therefore the stress intensity correction proposed in Equation 23 could be a function of the dimensions of the test specimen and its loading configuration [63]. In addition, Ebrahimi et al. [5, 6] have demonstrated that a non-linear compliance-crack length relationship exists for alumina because of crack bridging and R-curve phenomena. They demonstrated that by subtracting the R-curve effect, a unique v-K curve could be obtained for alumina with average grain size varying between 2 and 13 μm. Based on the corrections proposed and other results presented in the literature, we make practical recommendations for double torsion testing and suggest work that could lead to the standardization of this test technique.

9. Recommendations for double-torsion testing and future work

Researchers experienced with the practical aspects of double torsion testing recognize that good alignment is the key to successful application of this test method [3, 45]. A well

aligned loading fixture distributes torsion symmetrically in the two bars. A misaligned system, evidenced by cracks that do not run straight from the notch has uneven torsion in the bars resulting in mixed-mode loading of the crack, and results in artificially enhanced K_{IC} values. As mentioned earlier, the presence of a guiding groove modifies the real stress intensity factor at the crack tip and leads to uncertainty and inaccuracy in fracture toughness and slow crack growth measurement. Based on the present survey, it is recommended that machined grooves be avoided in all situations. Other experimental aspects that increase the repeatability of double-torsion testing are a stiff machine, test specimens machined to tight tolerances and with well finished surfaces, good environmental control, ball bearing loads, homogeneous material along crack extension region and a data acquisition system with high accuracy [33, 45, 81]. For slow crack growth studies via load relaxation, a high throughput data acquisition system may be necessary to accurately capture the rapid initial relaxation in loads resulting from high growth rates. There is agreement among researchers on machining a tapered notch on the test specimen in order to facilitate precracking at loads lower than the fracture load. As mentioned in Section 4, an important practical consideration in precracking is to allow the crack to reach the steady state front before conducting fracture toughness or slow crack growth measurements [63].

It is important to use high loading/displacement rates during fracture toughness determination [54]. This is especially important for materials which are susceptible to slow crack growth. For slow crack growth studies, it is helpful to know the fast fracture load of a test beforehand so that load relaxation tests can be carried out by arresting the crosshead at a load such that $K > 0.9\ K_{IC}$ [33, 60]. Caution should be exercised when interpreting crack growth data obtained from load relaxation alone especially at elevated temperatures and/or at very low velocities ($<10^{-7}$ m/s) [44]. It is advised that the slow crack growth behavior of a material can be evaluated by using a combination of the load relaxation and the constant load or the constant displacement rate techniques [56]. It is also helpful to obtain an experimental compliance-crack length curve from at least six to eight test specimens with different initial crack lengths [25, 85]. Apart from providing scaling constants for accurate crack velocity determination, these results also provide an estimate of the deviation between the theoretical compliance and its experimental value based on the load train and test specimen geometry.

It is to be noted that the double-torsion testing procedure only gives information for the crack propagation behavior of macro-flaws. This test method therefore, can not be directly applied to lifetime prediction in cases where the growth of micro-flaws constitutes a significant portion of the total lifetime. One area where the potential of the double-torsion method has not been fully utilized is to obtain *R*-curve behavior and bridging stresses of materials [4–6]. As noted earlier, bridging stresses cause the compliance versus crack length calibration of double-torsion test specimens to become non-linear [5]. If accurate *R*-curve behavior is obtained, the slow crack growth behavior of micro-cracks can be indirectly estimated with the double-torsion testing technique by subtracting the possible effect of the reinforcements on macro-cracks. The information generated by the double-torsion testing procedure can therefore, be applied to component life prediction.

In the absence of standardized guidelines, double-torsion test specimens of different dimensions have been used for fracture investigations. Tait, Fry and Garrett [45] surveyed the test specimen dimensions for published data in the literature and concluded that a length to width ratio of two to three has been a popular choice. *A* length to width ratio of two gives less material in the middle for slow crack growth experiments. Longer length to width ratios may be applied for slow crack growth studies in order to increase the size of the region with nearly constant stress intensity. That survey [45] also found that the thickness values of the test specimen typically lie between 1/6 and 1/15 of the test specimen width. Test specimens thicker than *S*/6 should be avoided since it leads to experimental complications such as those arising from an interaction between the torsion bars. It is the opinion of the authors that detailed finite element studies on ungrooved test specimens with sizes typical of double-torsion test specimens in practice are required to design a standardized test specimen with well-defined constant stress intensity region. The fracture modality, i.e., whether plane stress or plane strain expression for stress intensity factor in Equation 8 is applicable, should also be addressed for the standard specimen design. Efforts to compare the fracture toughness results from double-torsion and other standardized test methods (e.g., ASTM's C1421) are under way. These studies coupled with round-robin testing among laboratories are important steps towards standardization of this test procedure.

10. Concluding remarks

The double-torsion testing methodology is a simple, yet powerful test method to characterize the fracture behavior of materials and the applicability of this test method is not limited as long as its limitations are addressed appropriately. The authors believe that because of its attributes and popularity, efforts should be focused on the standardization of this test method.

Acknowledgements

This work was sponsored by the U.S. Department of Energy, Assistant Secretary for Energy Efficiency and Renewable Energy, Office of FreedomCAR and Vehicle Technology Program, as part of the Heavy Vehicle Propulsion Materials Program, under contract DE-AC05-00OR22725 with UT-Battelle, LLC. The authors would like to thank the anonymous reviewers and their colleague Donald Erdman (ORNL) for many insightful comments.

The authors are indebted to George D. Quinn (NIST) for bringing a number of references to their attention and for reviewing the manuscript and offering many valuable suggestions

References

1. J. O. OUTWATER and D. J. GERRY, *J. Adhesion* **1** (1969) 290.
2. J. A. KIES and B. J. CLARK, in "Fracture—1969," edited by P. L. PRATT (Chapman & Hall, London, 1969) p. 483.
3. G. D. QUINN, *J. Mater. Sci.* **22** (1987) 2309.
4. G. VENIKIS, M. F. ASHBY and P. W. R. BEAUMONT, *Acta Metall. Mater.* **38** (1990) 1151.
5. M. E. EBRAHIMI, J. CHEVALIER and G. FANTOZZI, *J. Eur. Ceram. Soc.* **23** (2003) 943.
6. M. E. EBRAHIMI, J. CHEVALIER and G. FANTOZZI, *J. Mater. Res.* **15** (2000) 142.
7. L. GREMILLARD, T. EPICIER, J. CHEVALIER and G. FANTOZZI, *Acta Mater.* **48** (2000) 4647.
8. L. GREMILLARD, J. CHEVALIER, T. EPICIER and G. FANTOZZI, *J. Am. Ceram. Soc.* **85** (2002) 401.
9. C. BENAQQA, J. CHEVALIER, M. SAADAOUI and G. FANTOZZI, *Key Eng. Mater.* **206–213** (2002) 1641.
10. H. RHANIM, C. OLAGNON, G. FANTOZZI and R. TORRECILLAS, *Ceram. Int.* **23** (1997) 497.
11. *Idem., J. Eur. Ceram. Soc.* **17** (1997) 85.
12. R. K. GOVILA, *J. Am. Ceram. Soc.* **63** (1980) 319.
13. K. D. MCHENRY, T. YONUSHONIS and R. E. TRESSLER, *J. Am. Ceram. Soc.* **59** (1976) 262.
14. S. BASKARAN, S. B. BHADURI and D. P. H. HASSELMAN, *J. Am. Ceram. Soc.* **68** (1985) 112.
15. K. D. MCHENRY and R. E. TRESSLER, *J. Am. Ceram. Soc.* **63** (1980) 152.
16. H. RICHTER, G. KLEER, W. HEIDER and R. ROTTENBACHER, *Mater. Sci. Eng.* **71** (1985) 203.
17. K. D. MCHENRY and R. E. TRESSLER, *Am. Ceram. Soc. Bull.* **59** (1980) 459.
18. S. B. BHADURI, *Mater. Lett.* **12** (1991) 373.
19. R. FRASSINE, *J. Comp. Mater.* **26** (1992) 1339.
20. R. FRASSINE, M. RINK and A. PAVAN, *J. Comp. Mater.* **27** (1993) 921.
21. R. FRASSINE and A. PAVAN, *Comp. Sci. Tech.* **54** (1995) 193.
22. R. FRASSINE, M. RINK and A. PAVAN, *ibid.* **56** (1996) 1253.
23. R. HILL and C. STYLES, *J. Mater. Sci. Lett.* **11** (1992) 1555.
24. N. SRIDHAR, J. A. KARGOL and N. F. FIORE, *Scripta Metall.* **14** (1980) 225.
25. D. P. WILLIAMS and A. G. EVANS, *J. Test. Eval.* **1** (1973) 264.
26. R. P. BURFORD and A. POTOK, *J. Mater. Sci.* **22** (1987) 1651.
27. R. FRASSINE, T. RICCO, M. RINK and A. PAVAN, *ibid.* **23** (1988) 4027.
28. D. M. KULAWANSA, S. C. LANGFORD and J. T. DICKISON, *J. Mater. Res.* **7** (1992) 1292.
29. B. G. EGAN and O. DELATYCKI, *J. Mater. Sci. Lett.* **14** (1995) 340.
30. T. RICCO, R. FRASSINE and A. PAVAN, *J. Mater. Sci.* **25** (1990) 1517.
31. T. LIN, G. A. COOPER and M. HOOD, *ibid.* **29** (1994) 4750.
32. M. CICCOTTI, N. NEGRI, G. GONZATO and F. MULARGIA, *Int. J. Rock Mech. Min. Sci.* **38** (2001) 569.
33. M. CICCOTTI, N. NEGRI, L. SASSI, G. GONZATO and F. MULARGIA, *J. Volcan. Geotherm. Res.* **98** (2000) 209.
34. P. G. MEREDITH and B. K. ATKINSON, *Phys. Earth Planetary Sci.* **39** (1985) 33.
35. M. SAADAOUI, P. REYNAUD, G. FANTOZZI, F. PERONNET and J. P. CASPAR, *Ceram. Int.* **26** (2000) 435.
36. P. FRANKLIN, D. J. WOOD and N. L. BUBB, *Dent. Mater.* **21** (2005) 365.
37. D. J. INDRANI, W. D. COOK, F. TELEVANTOS, M. J. TYAS and J. K. HARCOURT, *ibid.* **11** (1995) 201.
38. M. A. H. DONNERS, L. J. M. G. DORTMANS and G. DE WITH, *J. Mater. Res.* **15** (2000) 1377.
39. M. A. H. DONNERS, L. J. M. G. DORTMANS, G. DE WITH and M. DE GRAEF, *Key Eng. Mater.* **132–136** (1997) 714.
40. M. RADOVIC and E. LARA-CURZIO, *Acta Mater.* **52** (2004) 5747.
41. P. J. MCAULIFFE and R. W. TRUSS, *J. Mater. Sci.: Mater. Med.* **5** (1994) 138.
42. A. R. DAVIES, J. E. FIELD, K. TAKAHASHI and K. HADA, *Diamond Rel. Mater.* **14** (2005) 6.
43. E. R. FULLER JR, in "Fracture Mechanics Applied to Brittle Materials—ASTM STP 678", edited by S. W. FREIMAN (American Society for Testing and Materials, 1979) p. 3.
44. B. J. PLETKA, E. R. FULLER JR and B. G. KOEPKE, in "Fracture Mechanics Applied to Brittle Materials—ASTM STP 678", edited by S. W. FREIMAN (American Society for Testing and Materials, 1979) p. 19.
45. R. B. TAIT, P. R. FRY and G. G. GARRETT, *Exp. Mech.* **27** (1987) 14.
46. A. G. EVANS, *J. Mater. Sci.* **7** (1972) 1137.
47. M. CICCOTTI, *J. Am. Ceram. Soc.* **83** (2000) 2737.
48. J. M. GERE and S. P. TIMOSHENKO, in "Mechanics of Materials" (PWS Publishing Company, Boston, MA, 1997) p. 192.
49. D. R. BISWAS and V. K. PUJARI, *J. Am. Ceram. Soc.* **64** (1981) C98.
50. T. L. ANDERSON, in "Fracture Mechanics: Fundamentals and Applications" (CRC Press, New York, NY, 1994) p. 31.
51. G. G. TRANTINA, *J. Am. Ceram. Soc.* **60** (1977) 338.
52. M. CICCOTTI, G. GONZATO and F. MULARGIA, *Int. J. Rock Mech. Min. Sci.* **37** (2000) 1103.
53. S. DEVILLE, H. E. ATTAOUI and J. CHEVALIER, *J. Eur. Ceram. Soc.* **25** (2005) 3089.
54. A. SELCUK and A. ATKINSON, *J. Am. Ceram. Soc.* **83** (2000) 2029.
55. C. S. MARTINS, M. STEEN and L. G. ROSA, *J. Test. Eval.* **19** (1991) 256.
56. O. SANO, *J. Mater. Sci.* **23** (1988) 2505.
57. H. R. MCKINNEY and H. L. SMITH, *Am. Ceram. Soc. Bull.* **50** (1971) 784.
58. S. M. WEIDERHORN in "Fracture Mechanics of Ceramics," edited by R. C. Bradt, D. P. H. Hasselman, and F. F. Lange (Plenum Press, New York, 1974) Vol. 2, p. 613.
59. G. D. QUINN and J. B. QUINN, in "Fracture Mechanics of Ceramics," edited by R. C. Bradt, A. G. Evans, D. P. H. Hasselman and F. F. Lange (Plenum Press, New York, 1983) Vol. 6 p. 603.
60. P. R. FRY and G. G. GARRETT, *J. Mater. Sci.* **23** (1988) 2325.
61. J. CHEVALIER, C. OLAGNON and G. FANTOZZI, *J. Am. Ceram. Soc.* **82** (1999) 3129.
62. P. ZHU, Z. LIN, G. CHEN and I. KIYOHIKO, *Int. J. Fatigue* **26** (2004) 1109.
63. J. CHEVALIER, M. SAADAOUI, C. OLAGNON and G. FANTOZZI, *Ceram. Int.* **22** (1996) 171.
64. J. CHEVALIER, C. OLAGNON, G. FANTOZZI and B. CALES, *ibid.* **23** (1997) 263.
65. *Idem., J. Am. Ceram. Soc.* **78** (1995) 1889.
66. J. CHEVALIER, C. OLAGNON, G. FANTOZZI, J. M. DROUIN and B. CALES, *Key Eng. Mater.* **132–136** (1997) 512.
67. J. CHEVALIER, A. H. DEAZA, L. GREMILLARD, R. ZENATI and G. FANTOZZI, *Mater. Eng.* **12** (2001) 159.
68. A. H. DEAZA, J. CHEVALIER, G. FANTOZZI, M. SCHEHL and R. TORRECILLAS, *J. Am. Ceram. Soc.* **86** (2003) 115.
69. *Idem., Key Eng. Mater.* **206–213** (2002) 1535.
70. S. M. LEE, *J. Comp. Mater.* **20** (1986) 185.
71. A. C. MALONEY, H. H. KAUSCH and H. R. STIEGER, *J. Mater. Sci. Lett.* **3** (1984) 776.

72. C.-D. QIN, N. A. JAMES and B. DERBY, *Acta Metall. Mater.* **40** (1990) 925.
73. A. V. VIRKAR and D. L. JOHNSON, *J. Am. Ceram. Soc.* **59** (1976) 197.
74. C. COLIN, M. BOUSSUGE, D. VALENTIN and G. DESPLANCHES, *J. Mater. Sci.* **23** (1988) 2121.
75. B. J. DALGLEISH, P. L. PRATT, R. D. RAWLINGS and A. FAKHR, *Mater. Sci. Eng.* **45** (1980) 9.
76. J. L. ROUTBORT and H. MATZKE, *J. Mater. Sci.* **18** (1983) 1491.
77. A. BRIGGS, R. AIREY and B. C. EDWARDS, *ibid.* **16** (1981) 125.
78. F. SUDREAU, C. OLAGNON and G. FANTOZZI, *Ceram. Int.* **20** (1994) 125.
79. B. J. PLETKA and S. M. WIEDERHORN, *J. Mater. Sci.* **17** (1982) 1247.
80. M. K. FERBER and S. D. BROWN, *J. Am. Ceram. Soc.* **63** (1980) 424.
81. L. LI and R. F. PABST, *J. Mater. Sci.* **15** (1980) 2861.
82. R. F. PABST and J. WEICK, *J. Mater. Sci. Lett.* **16** (1981) 836.
83. A. V. VIRKAR and R. S. GORDON, *J. Am. Ceram. Soc.* **58** (1975) 536.
84. J. C. POLLET and S. J. BURNS, *ibid.* **62** (1979) 426.
85. R. KAHRAMAN, J. F. MANDELL and M. C. DEIBERT, *ibid.* **80** (1997) 1812.
86. D. K. SHETTY and A. V. VIRKAR, *ibid.* **61** (1978) 93.
87. N. E. PRASAD and S. B. BHADURI, *J. Mater. Sci.* **23** (1988) 3106.
88. D. K. SHETTY, A. V. VIRKAR and M. B. HARWARD, *J. Am. Ceram. Soc.* **62** (1979) 307.
89. P. J. HINE, R. A. DUCKETT and I. M. WARD, *J. Mater. Sci.* **19** (1984) 3796.
90. P. S. LEEVERS, *J. Mater. Sci.* **17** (1982) 2469.
91. P. S. LEEVERS, *J. Mater. Sci. Lett.* **5** (1986) 191.
92. A. H. DEAZA, J. CHEVALIER, G. FANTOZZI, M. SCHEHL and R. TORRECILLAS, *Biomater.* **23** (2002) 937.

Received 14 June
and accepted 7 November 2005